2

UCRL-86911
PREPRINT

CONF-820119--2

UCRL--86911

DE82 006859

MASTER

ARGUS Laser-Plasma Experiments at 1.06μm, 0.53μm, and 0.35μm

R. E. Turner
E. M. Campbell
W. C. Mead
F. Ze
C. Max
D. W. Phillion
P. Lee
B. Pruett
G. Tirsell
B. F. Lasinski

This paper was prepared for submittal to
15th European Conference on Laser Interaction
with Matter
(ECLIM)
Schliersee, West Germany

January 18-22, 1982

Lawrence Livermore National Laboratory

Reg

DISCLAIMER

ARGUS Laser Plasma Experiments at 1.06μm, 0.53μm and 0.35μm

R. E. Turner, E. M. Campbell, W. C. Mead, F. Ze, C. Max
D. W. Phillion, P. Lee, B. Pruett, G. Tirsell, B. F. Lasinski

Lawrence Livermore National Laboratory
Livermore, California

ARGUS wavelength scaling experiments have been performed on low (Be) and high (Au) Z disk targets, with laser wavelengths of 1.06μm, 0.53μm and 0.35μm. The laser provided a 700 psec pulse, with up to 100J at 1.06μm; 200J at 0.53μm; and 40J at 0.35μm. Laser intensities on target ranged from 3×10^{13} to over $3 \times 10^{15} W/cm^2$, using an f/2.2 focusing system. Box calorimeter measurements show the expected increasing fractional absorption at shorter laser wavelengths; absolutely calibrated hard x-ray detectors show the number of suprathermal electrons to be greatly decreased. Scattered light measurements concentrated on stimulated Raman scattering, and the 3/2 harmonic. The SRS was spectrally and temporally resolved during 0.53μm irradiations; our measurements showed the scattering to be principally from the convective instability, near tenth critical density. Near ω/2, a double peaked spectral feature is observed.

The time resolved data show a number of interesting features, which will be discussed.

---

*Work performed under the auspices of the U.S. Department of Energy by the Lawrence Livermore National Laboratory under contract number W7405ENG48.

Wavelength scaling measurements, using the Argus laser system to irradiate disk targets with 700 psec pulses at 1.06μm, 0.53μm, and 0.35μm, have recently been completed. While the experiments concentrated on soft and hard x-ray measurements, additional diagnostics, measuring scattered light, provided information about the various processes taking place in the underdense plasma. These diagnostics included absorption measurements, and temporally and spectrally resolved measurements near; (1) the laser wavelength for stimulated Brillouin scattering (SBS); (2) wavelengths of 1.2 to 2.2 times the laser wavelength for stimulated Raman scattering (SRS); (3) and near the second and three-halves laser harmonics. All the measurements were not obtained at all 3 laser wavelengths. In particular, the low levels of instability generation at 0.35μm limited observations at that wavelength.

Figures 1 and 2 show the laser light absorption for Au and Be disk targets at the various laser wavelengths. For the high Z targets, and for the shorter laser wavelengths, the results are consistent with inverse bremsstrahlung as the dominant absorption mechanism.

Figures 3a and 3b show the absolute level of hard x-rays detected from the high Z targets, for the various intensities and wavelengths. It is clear that the number of suprathermal electrons present is greatly reduced at shorter laser wavelengths. The increased collisional absorption at shorter wavelengths reduces the amount of laser energy available for resonance absorption, and increases the threshold for various parametric instabilities.

Electromagnetic radiation at the 3/2 harmonic of the laser frequency is indicative of plasma waves at the quarter critical density of the laser light. The harmonic may be generated by coalescence of three plasmons, or by the non-linear combining of a plasmon and an incident wavelength photon. The spectral features suggest that the plasma waves are generated by the two plasmon decay instability[1].

Experimentally, at an angle of 30^{o} to the laser beam, we observe two peaks (in 1.06μm experiments), one red shifted, the other blue shifted, as shown in Figures 4 and 5. The usual[2] explanation for this is that we are observing a directly backscattered ($\theta > \pi/2$) red shifted wave, and a forward scattered ($\theta < \pi/2$) blue shifted wave which has

reflected off of its critical surface (at 9/4 n_c). Evidence in support of this hypothesis includes the following observations. The blue shifted light is reduced in amplitude compared to the red, presumably due to absorption. In 0.53μm experiments, the blue shifted light is not observed, which is consistent with the higher collisionality of the plasma. In burn through experiments on thin plastic foils, in which 3/2 light is observed in the forward direction, it is the red-shifted peak which is reduced or completely absent. Similar observations have been reported by others[3]. Other evidence, however, points out the limitations of this one dimensional model. Three halves spectral measurements, looking for 90^0 scattered light, should, according to equations (1) and (2) (discussed below), show only one peak. However, measurements show two well separated peaks. At this time, we do not have an adequate explanation for this observation. In addition, Doppler shifts, refraction, Brillouin scattering, 3-dimensional effects, the finite f-number of the focusing lens, etc. are neglected. Because of these limitations and assumptions, it is difficult to determine the validity of the temperatures derived from this data.

Avrov[2], et.al., use a model where the plasmon wavenumber is that which gives the highest 2 ω_{pe} growth rate[1], but does not necessarily allow for phase matching with an incident photon. This model gives

$$\Delta\lambda = -22.7\ T_e \cos\theta \quad (\text{Å}) \qquad (1)$$

for the wavelength shift away from the exact 3/2 harmonic, where T_e is the electron temperature in keV, and θ the angle of the scattered light with respect to the incident laser light. The higher order (but momentum conserving) process of 3 plasmon coalescence is calculated to give (within 5%) the same results.

Barr[4] gives the wavelength shift from the exact 3/2 harmonic, for a 1.06μm laser, as

$$\Delta\lambda = -33.9\ T_e\ [\cos\theta - 0.919\ ] \quad (\text{Å}) \qquad (2)$$

This equation may be derived by demanding phase matching (momentum conservation) between an incident photon and a $2\text{-}\omega_{pe}$ generated phasmon, adding together to form 3/2 ω photon. We note that the plasmon must have a wavenumber which is small compared to the wavenumber which is expected near threshold[1].

Figure 6 shows the temperature inferred from equation (1) for Be, Ti, and Au disks irradiated at a nominal intensity of $1 \times 10^{15} W/cm^2$. Use of equation (2) would give one-third lower temperatures. The red peak-blue peak separation was used, rather than the absolute value of either peak, since this value is less sensitive to Doppler effect shifts. The absorbed energy for these shots is 16J for Be, 22.5J for Ti, and 30J for Au. This energy is partioned into heating the material, hydrodynamic expansion, and radiation. For the gold, radiative losses account for approximately 10 Joules. Hydrodynamaic losses were not measured, but are presumably highest for the low Z beryllium, and lowest for the gold. Thus, even after accounting for its radition losses, we expect gold to be hotter than the lower Z plasmas, due to its higher absorption. This expectation is confirmed by the data, although the absolute value of the temperature is somewhat lower than that predicted by simulations, or inferred from SBS measurements. No attempt has been made to remove Doppler shift effects from the data; this requires knowledge of the velocities at both $n_c/4$ and $9n_c/4$. Since we expect the lower density to have a higher velocity, Doppler effects should cause us to underestimate the temperature. In fact, the 90^o measurements, which are less sensitive to Doppler shifts, show a wider splitting (higher temperature) than the corresponding 30^o measurements.

Temporally and spectrally resolved measurements for stimulated Raman scattering (SRS) were obtained from 0.53μm laser wavelength experiments. Time-averaged spectra were obtained with finite channel detectors (5% bandwidth) for the 1.06μm experiments. We did not observe significant levels of SRS during experiments at 0.35μm. This is not unexpected, given the low intensities ($\leq 10^{15} W/cm^2$) and modest scale lengths of these particular experiments.

The spectra from 1.06μm experiments is qualitatively different

from the spectra obtained from 0.53μm experiments. Figure 7 shows the 1.06μm experiment SRS data. This data was obtained with two (800Å FWHM channels) detectors, and compiled over 6 shots. The data is shown for the detector which viewed the target normal, 30^{o} from the laser beam. The second detector was located 30^{o} above the target normal, out of the plane of polarization. This detector was unchanged during these shots; it monitored the shot to shot reproducibility, which was found to be good. Notice that little light was observed at wavelengths of 1.8μm or less. The peaked spectrum is consistent with the absolute Raman instability, shifted to the red as predicted by the Bohm-Gross term in the plasma wave dispersion equation, for an electron temperature of 2 to 5keV. The spectrum could also be the result of linear mode conversion of a plasma wave which has been generated by the two plasmon decay instability. This diagnostic had insufficient resolution to distinguish fine spectral details. However, there is clear evidence for plasma waves at $n_c/4$, and not at lower densities. (Convective SRS near 1.8μm has been observed on SHIVA experiments at higher intensities and larger spot sizes.)

The SRS results from the 0.53μm experiments contrast strongly with the 1.06μm results. Figure 8 shows the time integrated spectrum from a gold disk target irradiated by 29 Joules of green light. The laser spot was highly structured, with some regions receiving intensities of well over $10^{16}W/cm^2$. The spectrum shows the signature of the convective Raman instability; i.e., scattered light at wavelengths shorter than $2\lambda_o$. There is a weaker, additional scattered light signal seen at $2\lambda_o$ (1.064μm). This double peaked structure does not resemble the spectrum expected for SRS, rather, it appears similar to the 3/2 harmonic spectra (Figures 4 and 5). It may result from the re-conversion of two plasmon decay plasma waves.

Figures 9(a) and (b) show the time resolved Raman backscatter (i.e., back through the f/2 focusing lens) spectra for a gold disk irradiated with green light at an intensity of $\sim 5\times10^{15}W/cm^2$. The laser was focussed approximately 150μm in front of the target; thus the disk was irradiated by a diverging laser beam. Within the dynamic range of the

streak camera (the S-1 photocathode is an order of magnitude more sensitive at 800nm than at 1064nm) only the convective instability is observed. This light is generated in the very underdense regions of the plasma: $0.05 \leq n/n_c \leq 0.16$, for $T_e \sim 3$keV and backscatter. The time scale is correlated with the incident pulse, with zero being the peak of the incident pulse ($\pm$100psec). We observe no SRS until near the peak of the incident laser pulse; the scattering then continues until the end of the laser pulse. The delay in SRS onset may be due to the finite length of time necessary for the plasma density scale length near $0.1n_c$ to evolve to large enough values to allow the SRS to grow. It may also be due to being below threshold until the time of the peak intensity. In this case, the observation that SRS continues for 500-800 psec, while the laser pulse intensity falls over an order of magnitude, may be indicative of filamentation. It should be noted that the plasma expands toward the region of best focus in this experiment; this means that the plasma continues to interact with a high intensity laser beam as it expands. Due to the poor beam quality, geometric optics calculations yield poor estimates of the intensity in this region; it increases only modestly (factor of 2-4) at best focus.

We have observed, on some but not all of our disk experiments, a rapid (<100 psec) pulsation of the scattered light signal. This may be a signature of wave breaking, followed by re-growth of the plasma waves. Analysis of this aspect of the data has just begun.

Figure 9(c) shows the time integrated spectrum near $\omega_0/2$ for this gold disk experiment. The same double peaked spectrum as shown in Figure 8 is observed. We do not, as yet, have an explanation for this spectra.

Figure 10(a) and (b) show the time resolved SRS measurements from a Be disk irradiated at normal incidence. The spectrum and temporal behavior is qualitatively similar to the gold target results. Figure 10(c) shows the time integrated spectra near $\omega_0/2$ for a (different) Be disk, one oriented 30^0 from the laser beam (target normal in the direction of the light collector). Light near $\omega_0/2$ is not observed when the target normal is not oriented toward the light collector. This is an expected result, since refraction will cause this

light to be strongly collimated. (It originates very near its own critical surface, so refractive effects are strong.)

To summarize, scattered light measurements are useful laser plasma interaction diagnostics. In wavelength scaling experiments, they show the effects of increasing collisional absorption at shorter laser wavelengths. SRS and 3/2 harmonic measurements show the presence of plasma waves at $n_c/4$ and lower densities; time resolved scattered light measurements give us dynamic information regarding plasma conditions and instability formation.

References

1. C.S. Liu, M. N. Rosenbluth, Phys. Fluids 19, 967 (1976).

2. A. I. Avrov, et. al., Sov. Phys. JETP 45, 507 (1977).

3. P. D. Carter, S. M. L. Sim, E. R. Wooding, Optics Comm. 32, 443 (1980).

4. H. C. Barr, Rutherford Lab. Annual Report, Sec. 8.3.3 (1979).

Figure Captions

1. Laser light absorption at 1.06μm, 0.53μm, and 0.35μm for gold disk targets.

2. Laser light absorption at 1.06μm, 0.53μm and 0.35μm for Be disk targets.

3. (a)Hard x-ray flux from gold disk targets irradiated at 1.06μm and 0.53μm. (b) Hard x-ray flux from Al disks irradiated at 1.06μm and 0.35μm.

4. 3/2 harmonic spectra from gold disk.1.06μm laser.

5. 3/2 harmonic spectra from Be disk, 1.06μm laser.

6. Temperatures inferred from Equation (1) for 1.06μm experiments at $1 \times 10^{15} W/cm^2$. Doppler effects not deconvolved.

7. Raman light spectrum for gold disk target, 1.06μm experiment.

8. Raman light spectrum for gold disk target, 0.53μm experiment.

9. SRS spectra from gold disk target, 0.53μm experiment (a) false color contour plot of streak record. Signal at lower right is 1.06μm timing fiducial; t=0 corresponds to the peak of the laser pulse; (b) spectrally integrated time history and time integrated spectrum from (a) (sharp cut-off at 0.7μm is instrumental limit). (c) time integrated spectrum near $\omega_0/2$. Sharp peak at 1.064μm is due to residual unconverted laser light.

10. SRS spectra from Be disk target, 0.53μm experiment. (a) false color contour plot of streak record; (b) spectrally integrated time history, and temporally integrated spectrum; (c) time integrated spectrum near $\omega_0/2$ for a different Be target (see text).

$1\omega_o$, $2\omega_o$, AND $3\omega_o$ ABSORPTION – Au DISK TARGETS

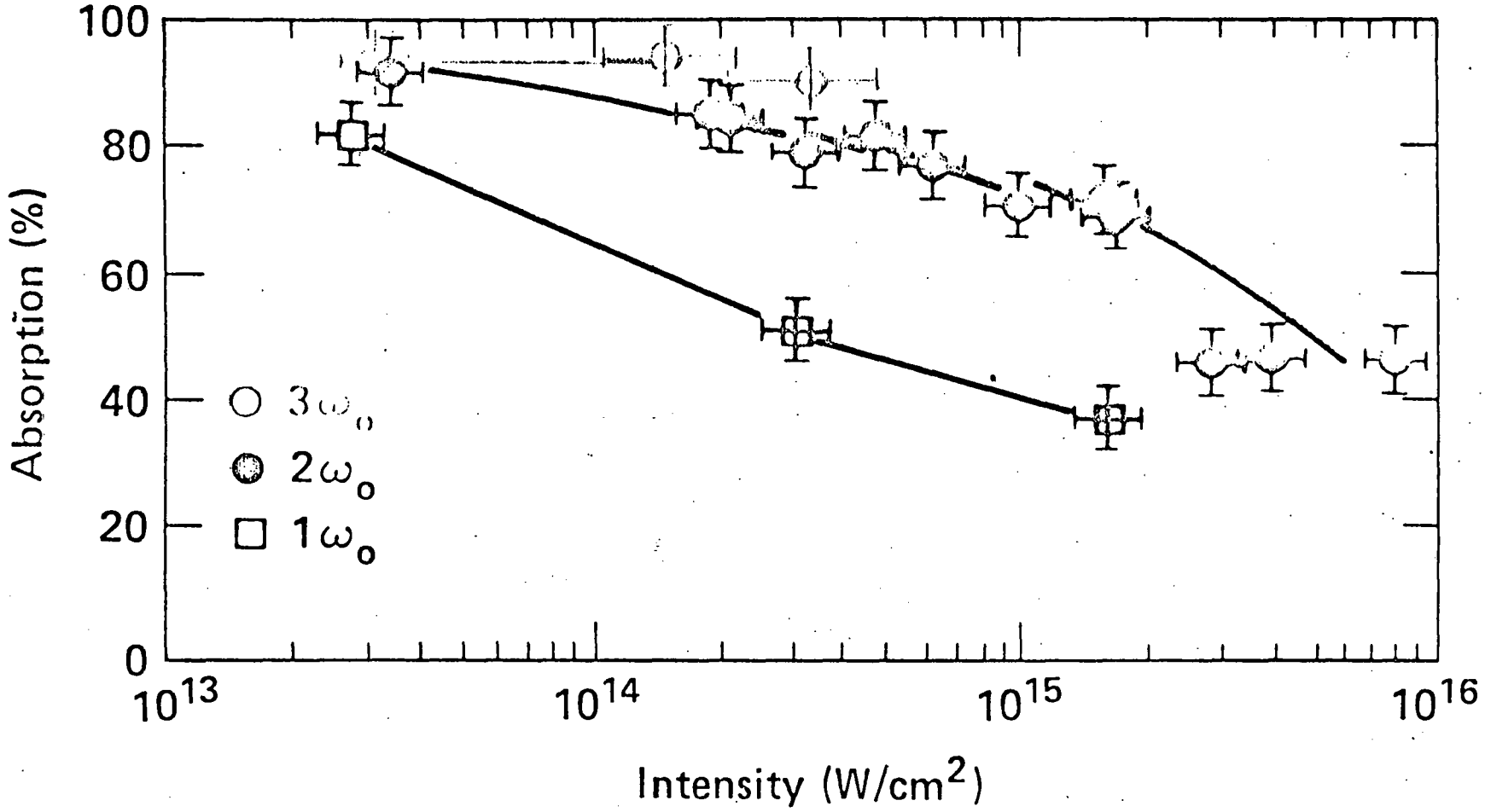

20-90-0381-0677

FIG 1

9/81

$1\omega_o$, $2\omega_o$, AND $3\omega_o$ ABSORPTION – Be DISK TARGETS

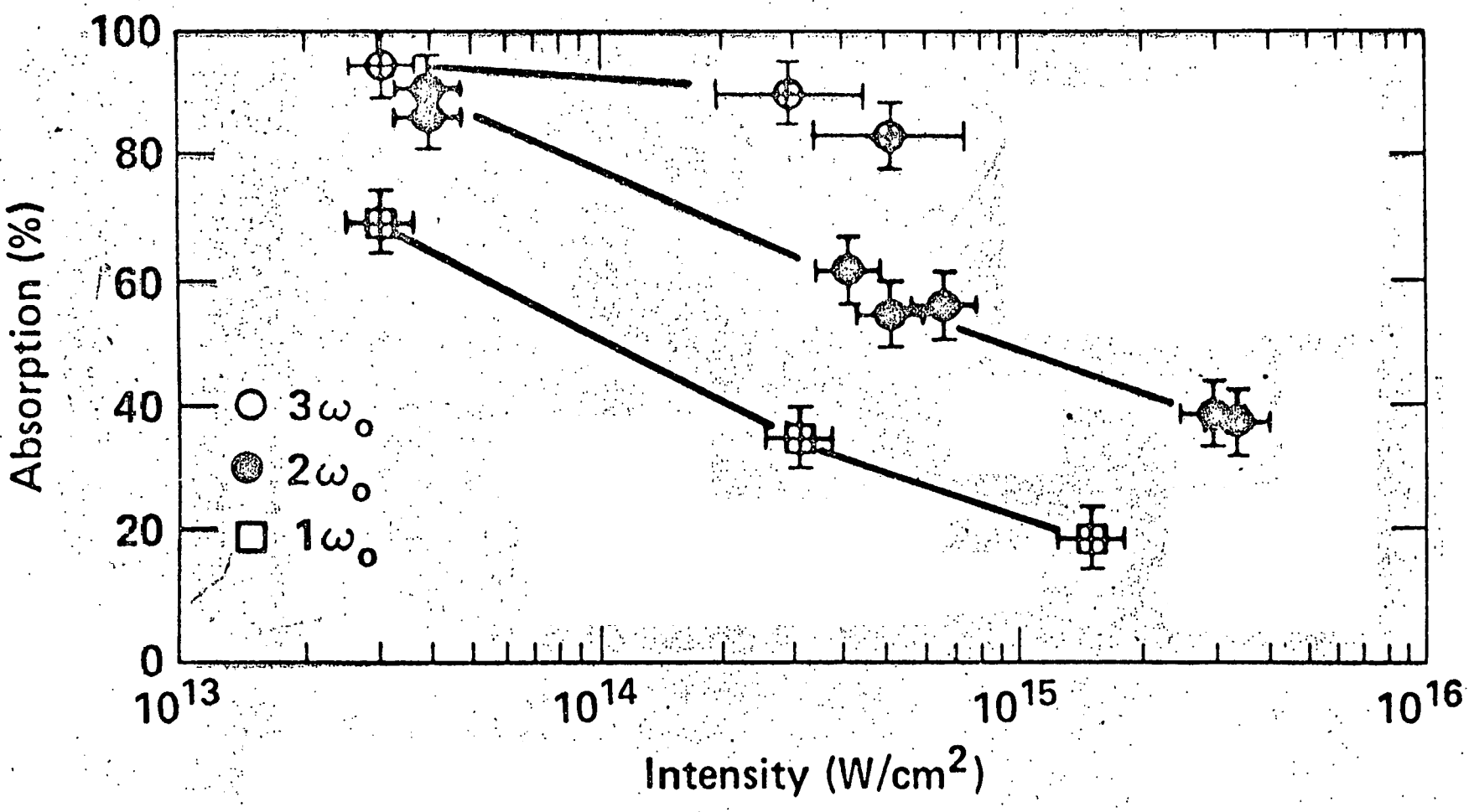

FIG 2

ARGUS WAVELENGTH SCALING

Supra thermal x-ray emission

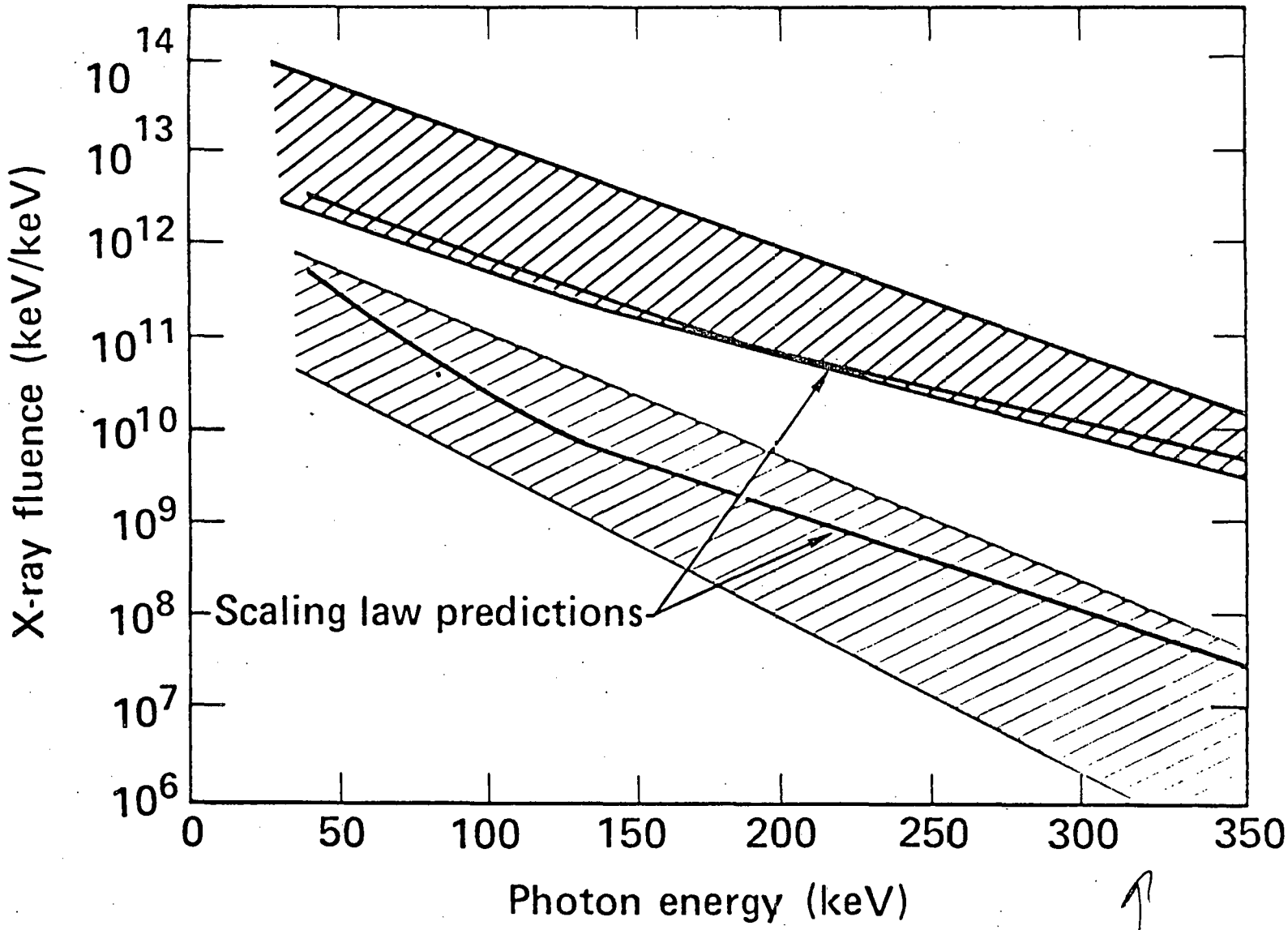

02-25-0881-2196

FIG 3 a & b

Similar to this: will show 3w data as well

TIME INTEGRATED 3/2 ω SPECTRUM

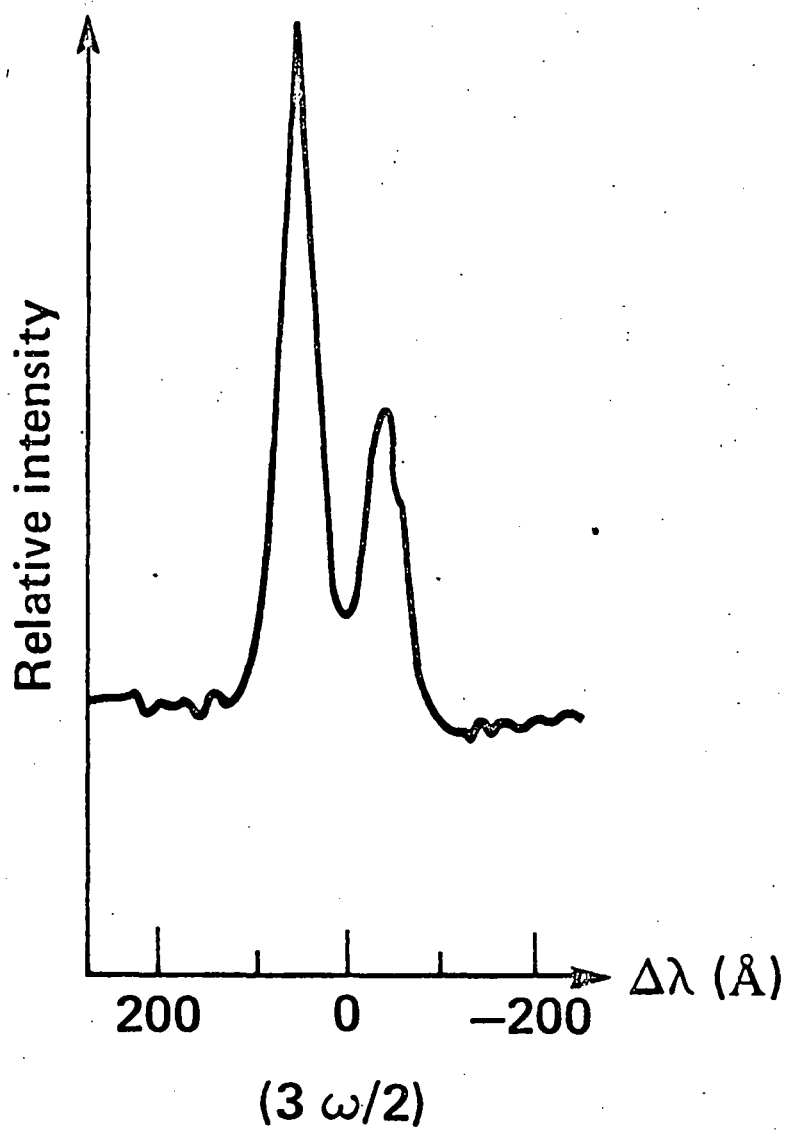

1.06 μm Experiment

$I = 1 \times 10^{15}$ W/cm^2 Au disk target

Red peak shifted ≈ 40 Å

Blue peak shifted ≈ 50 Å

20-90-1081-3199

FIG 4

TIME INTEGRATED 3/2ω SPECTRUM

$I = 3 \times 10^{14}$ W/cm^2 Be disk target

Red peak shifted ≈ 30 Å

Blue peak shifted ≈ 20 Å

1.06 μm Experiment

add

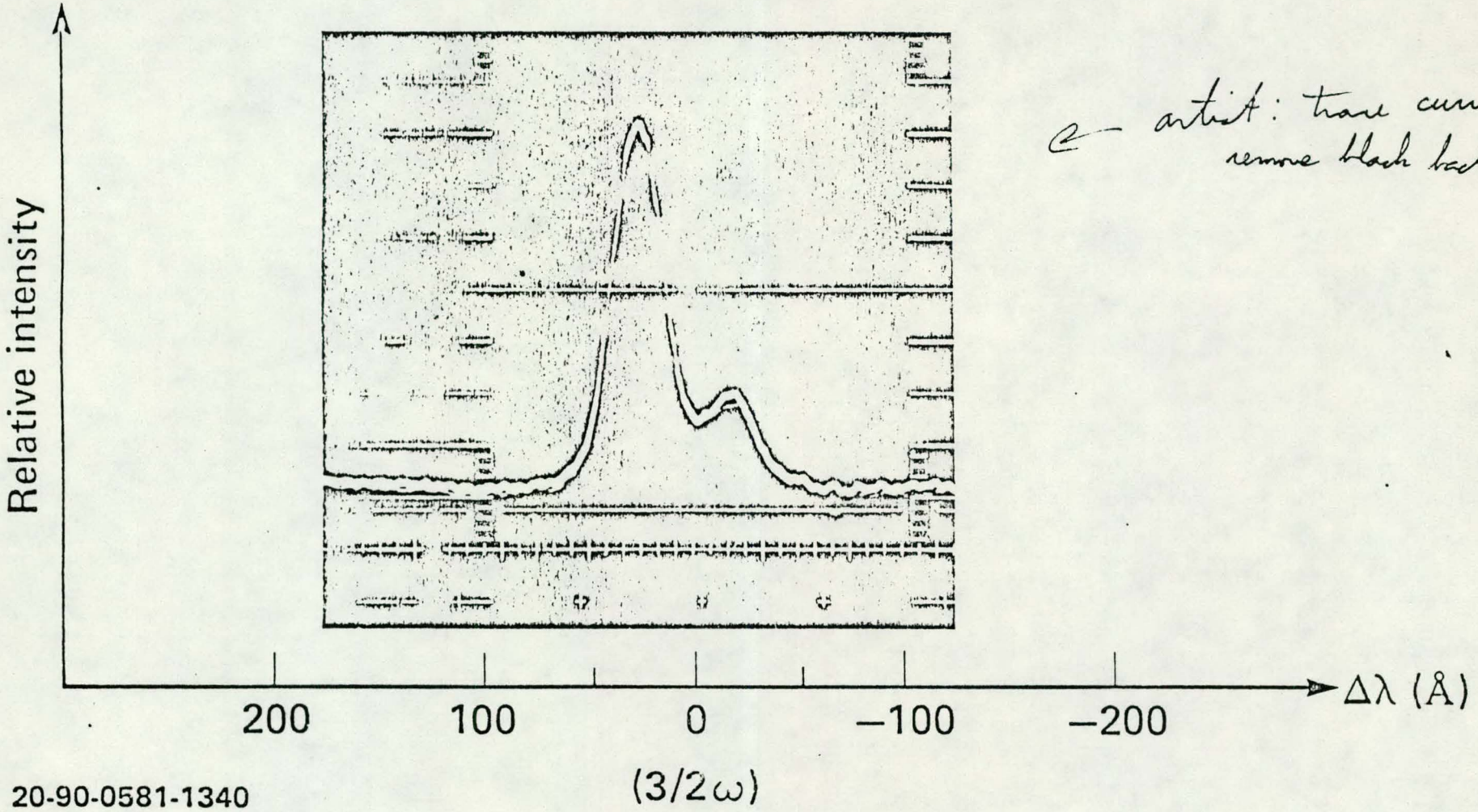

artist: trace curve remove black background

20-90-0581-1340

FIG 5

ELECTRON TEMPERATURES AT $n_c/4$ INFERRED FROM 3/2 HARMONIC SPECTRAL SPLITTINGS

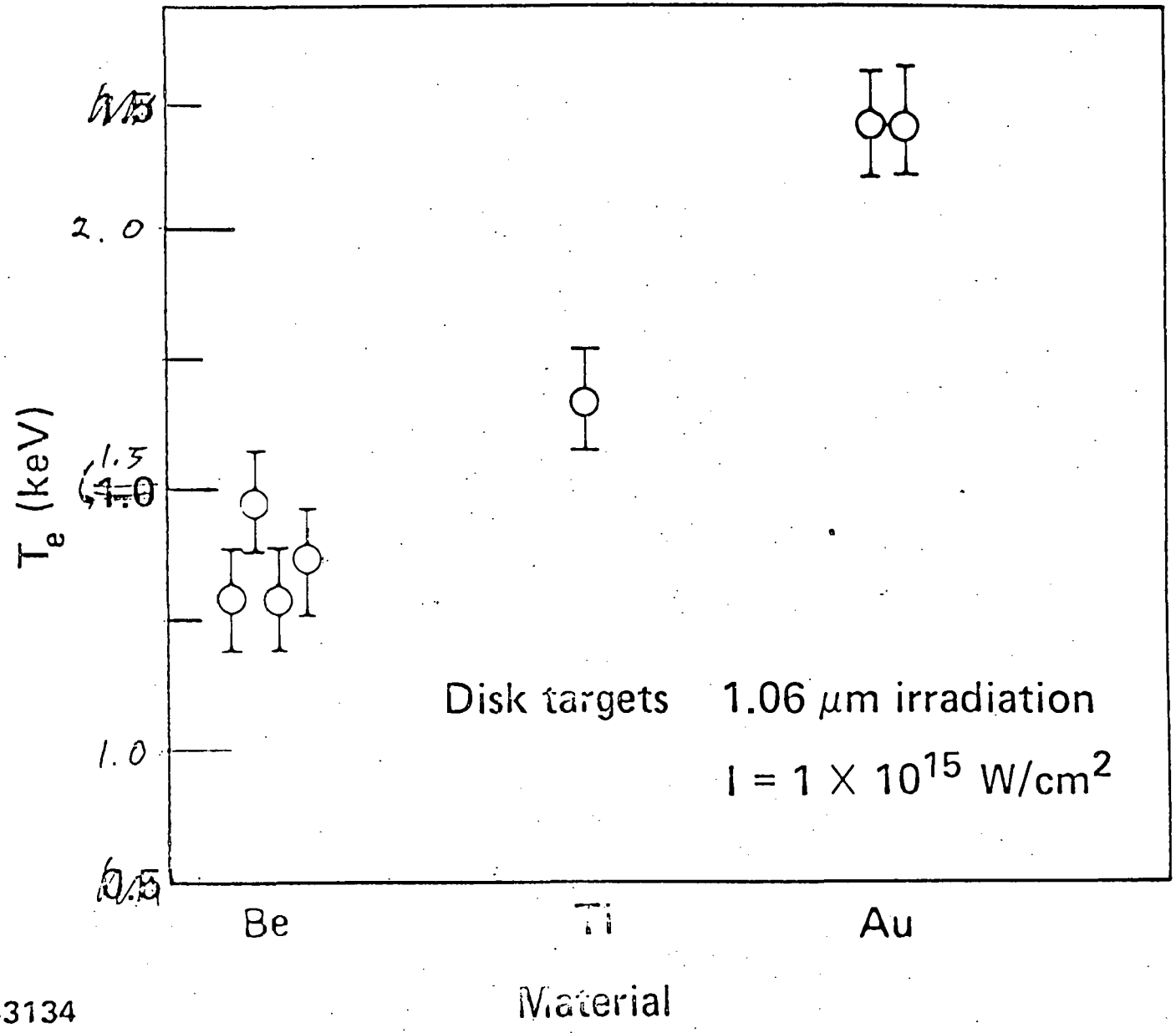

20-90-1081-3134

FIG 6

TIME INTEGRATED RAMAN SPECTRUM FROM Au DISK TARGETS

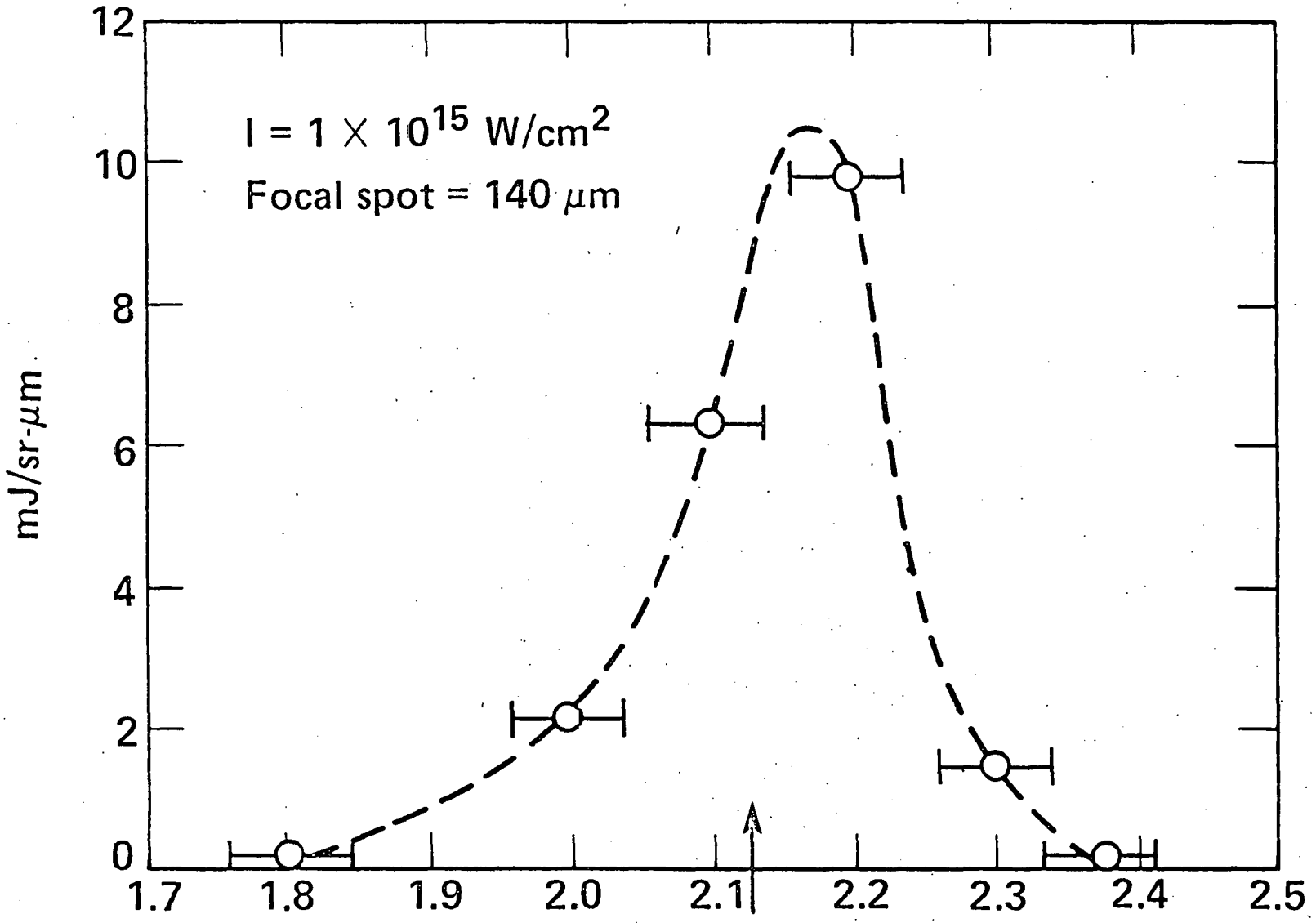

20-90-0581-1339

FIG 7

RAMAN LIGHT SPECTRUM FOR A DISK TARGET IRRADIATED WITH 5320 Å LIGHT

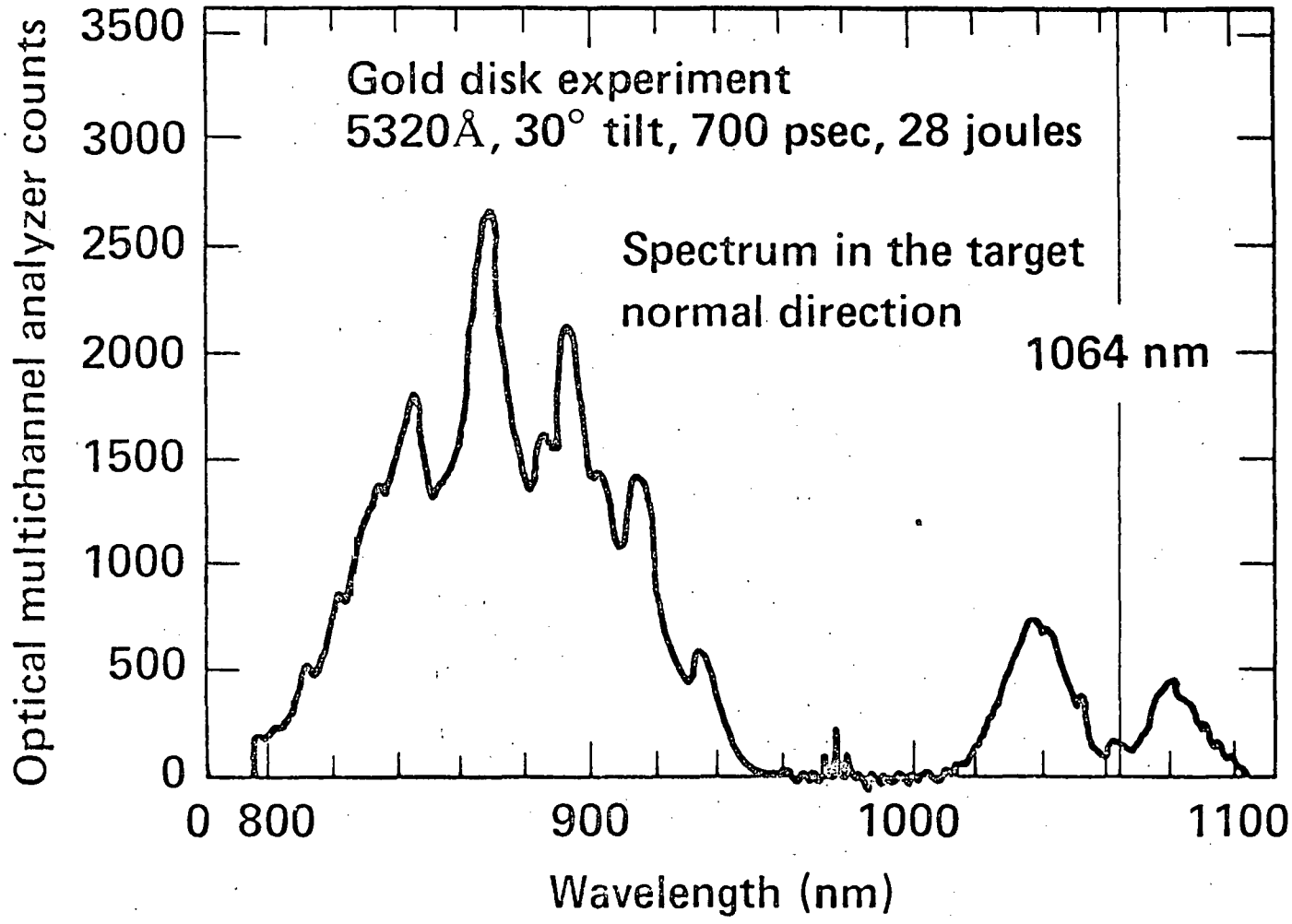

20-90-1081-3129

FIG 8

TIME-RESOLVED RAMAN-LIGHT SPECTRUM FOR A GOLD DISK IRRADIATED BY 5320 Å LASER LIGHT AT 5×10^{15} W/cm^2, 132 JOULES, 700 PSEC

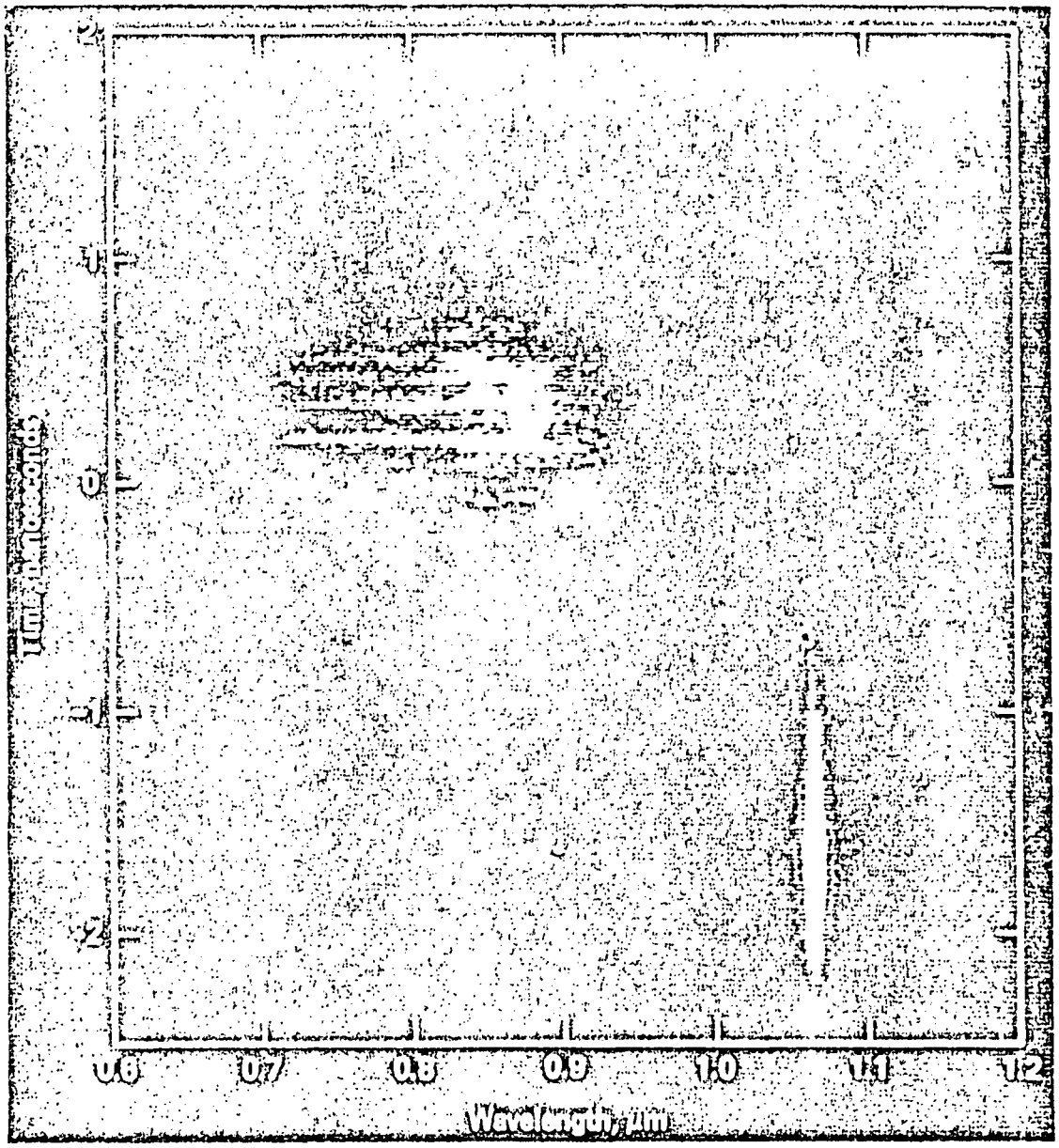

FIG 9(a)

TIME-RESOLVED RAMAN LIGHT SPECTRUM FOR A GOLD DISK IRRADIATED WITH 5320 Å LIGHT

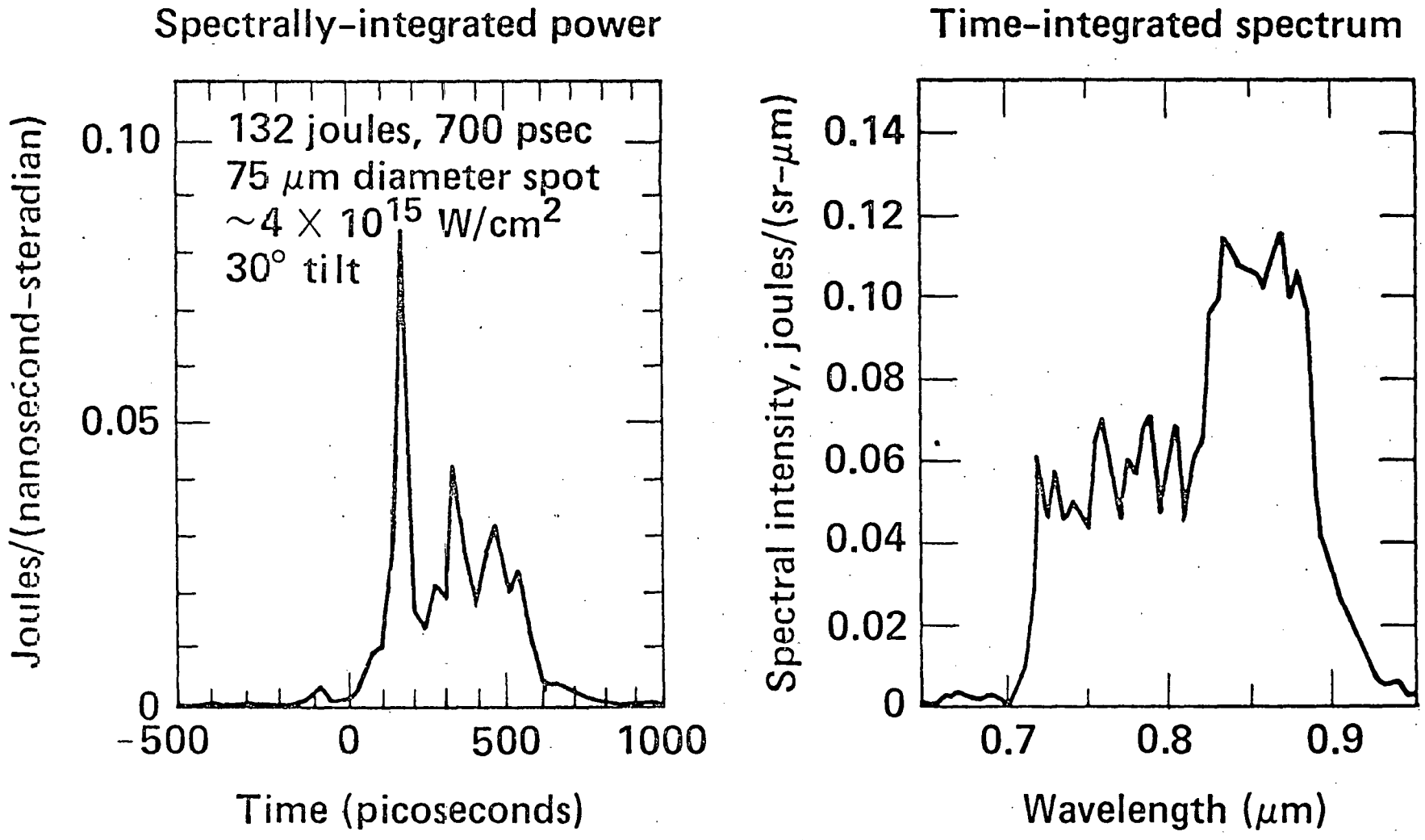

20-90-1081-3171

FIG 9(b)

SPECTRUM OF THE $\omega_0/2$ LIGHT FOR 5320 Å IRRADIATION OF A GOLD DISK

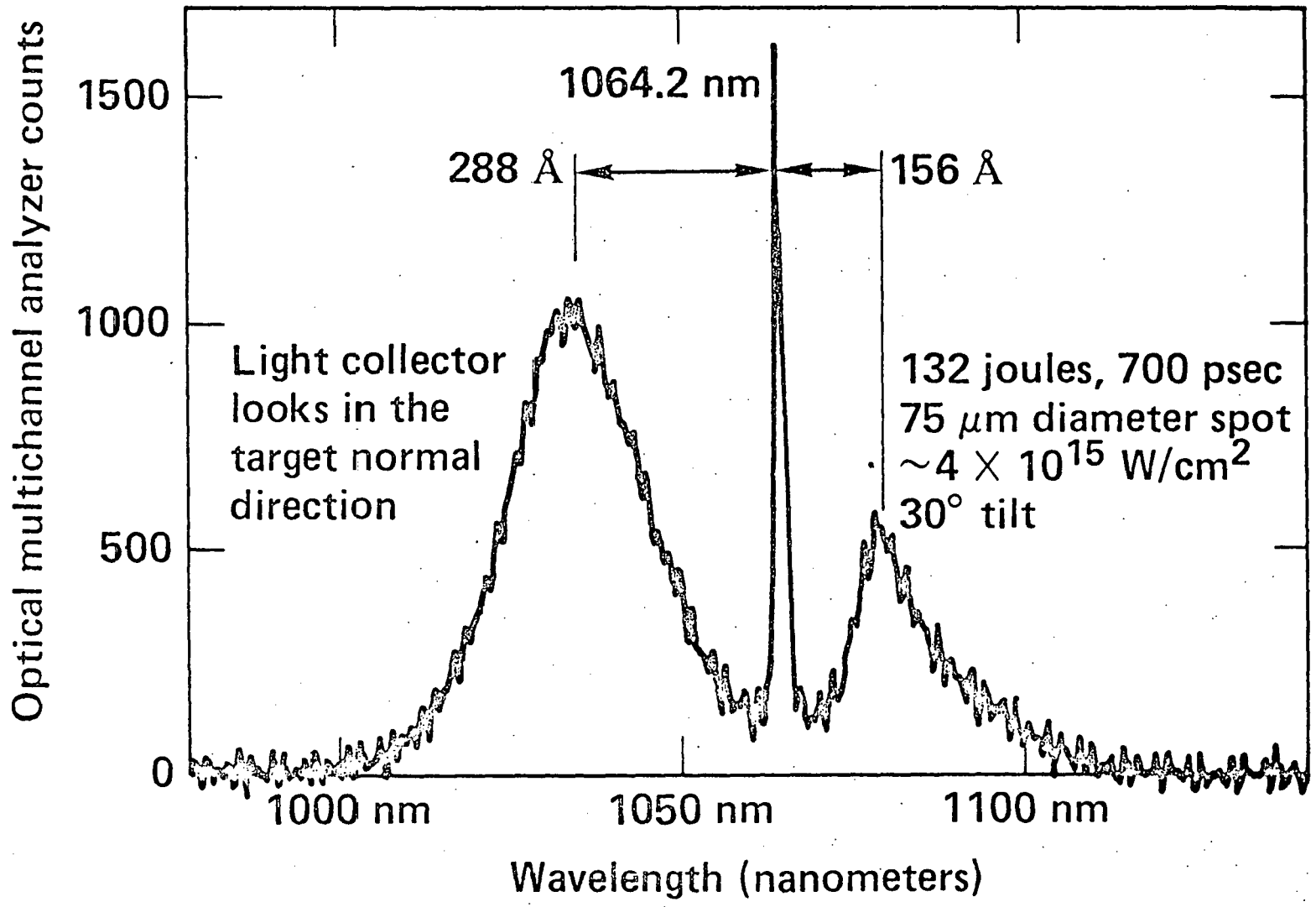

20-90-1081-3177

FIG 9(c)

TIME RESOLVED SPECTRUM FOR THE RAMAN LIGHT FOR 5320Å LASER IRRADIATION AT 5×10^{15} W/cm^2, 132 JOULES, 700 psec

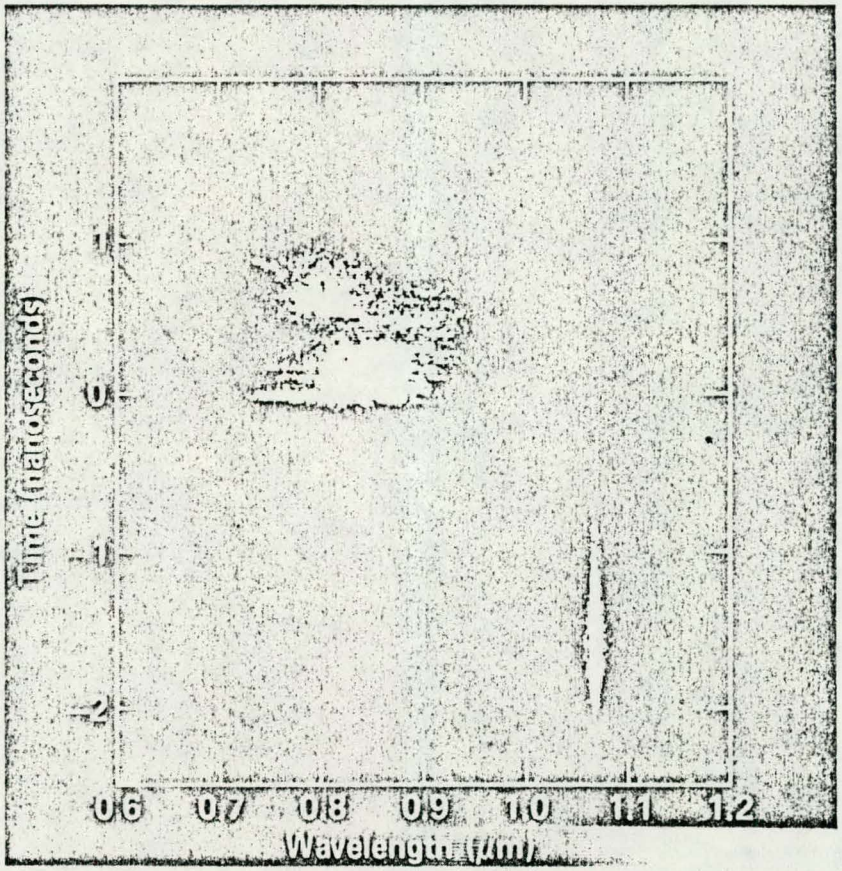

20-90-1081-3205

FIG 10(a)

TIME-RESOLVED RAMAN LIGHT SPECTRUM FOR A BERYLLIUM DISK IRRADIATED WITH 5320Å LIGHT

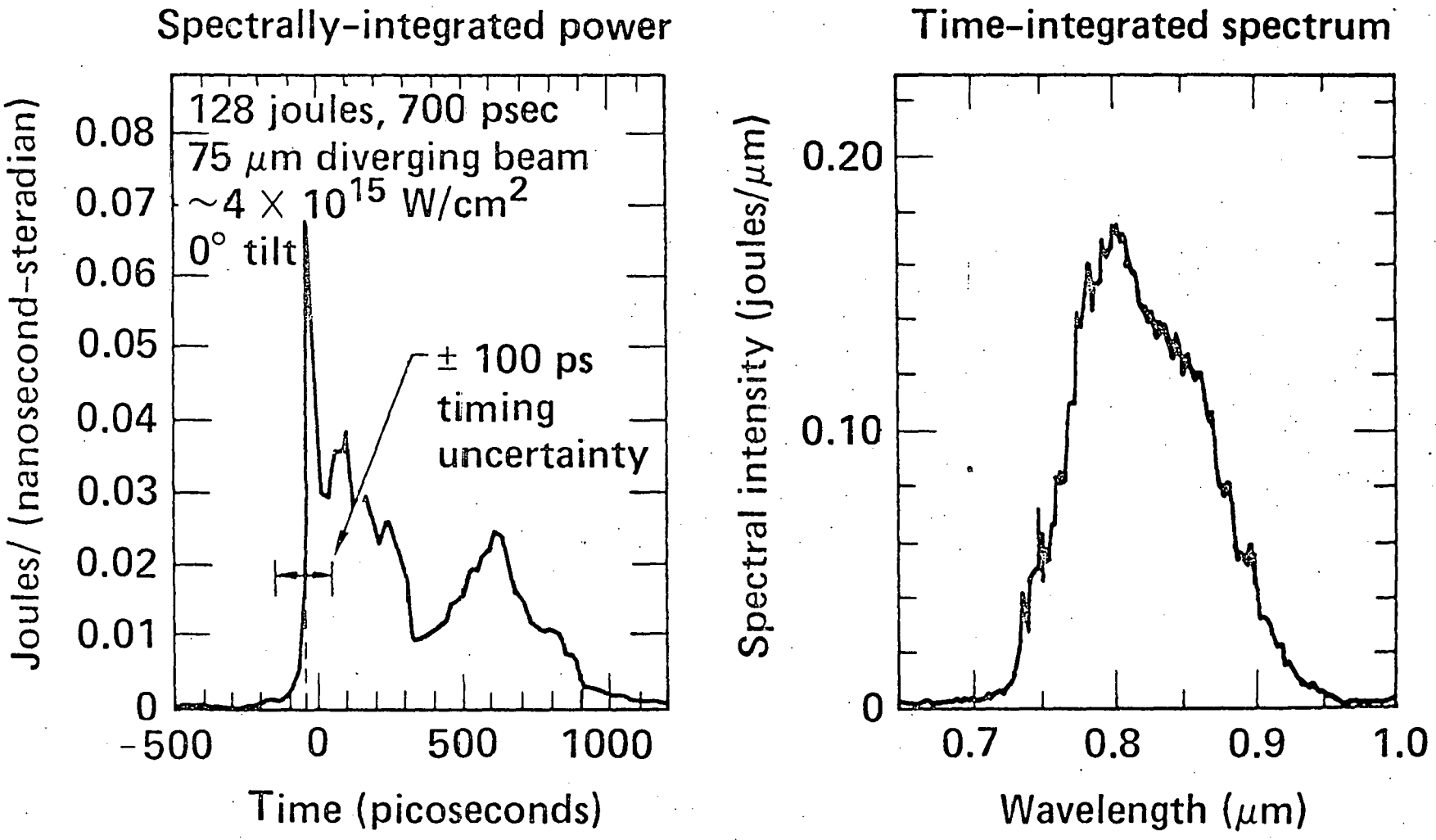

20-90-1081-3163

FIG 10(b)

SPLITTING OF THE $\omega_0/2$ LIGHT SPECTRUM IS MUCH LESS FOR A BERYLLIUM DISK THAN FOR A GOLD DISK FOR THE SAME IRRADIATION CONDITIONS

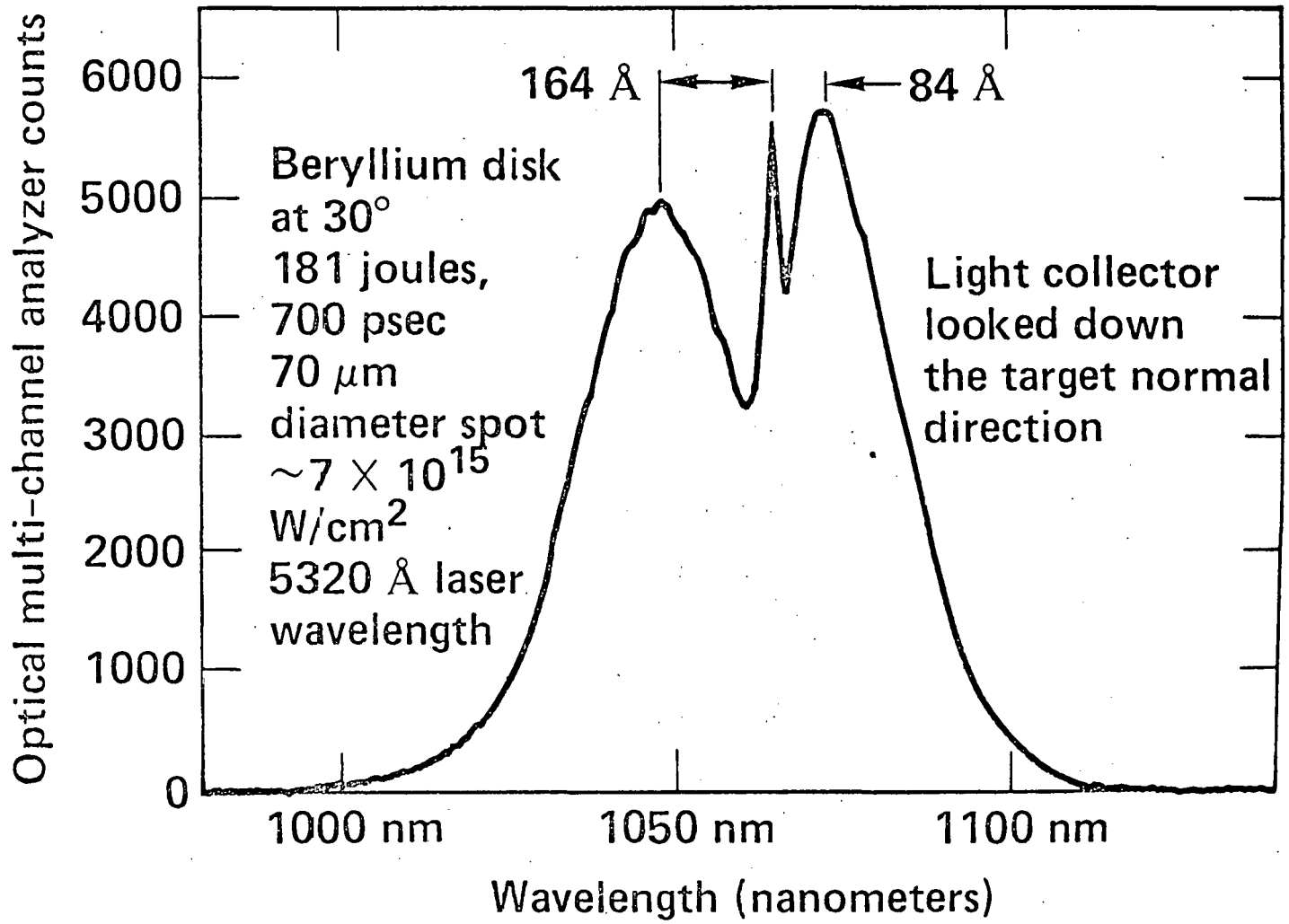

20-90-1081-3182

FIG 10(c)